iScience, Volume *23*

Supplemental Information

Coordination between Cell Motility and Cell Cycle Progression in Keratinocyte Sheets via Cell-Cell Adhesion and Rac1

Hiroaki Hirata, Oleg Dobrokhotov, and Masahiro Sokabe

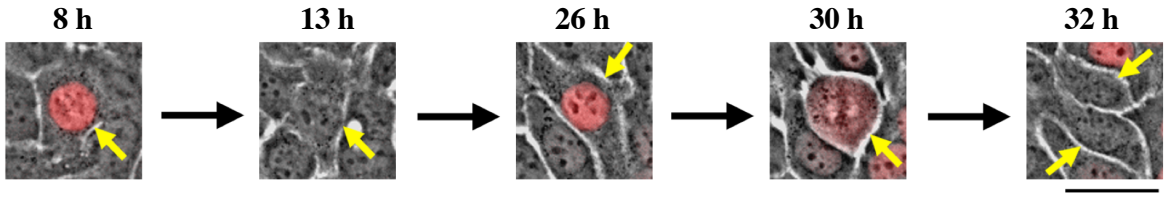

Figure S1. Time-dependent relationship between Geminin-based Fucci signal and cell division (Related to Figure 1). Geminin-based Fucci fluorescence images (red) overlaid to phase contrast images of a single cell and its daughter cells (yellow arrows) in a keratinocyte sheet at indicated time after seeding cells. Note that the Geminin signal at 8 h disappeared by 13-h time point without cell division. Scale bar: 30 μm.

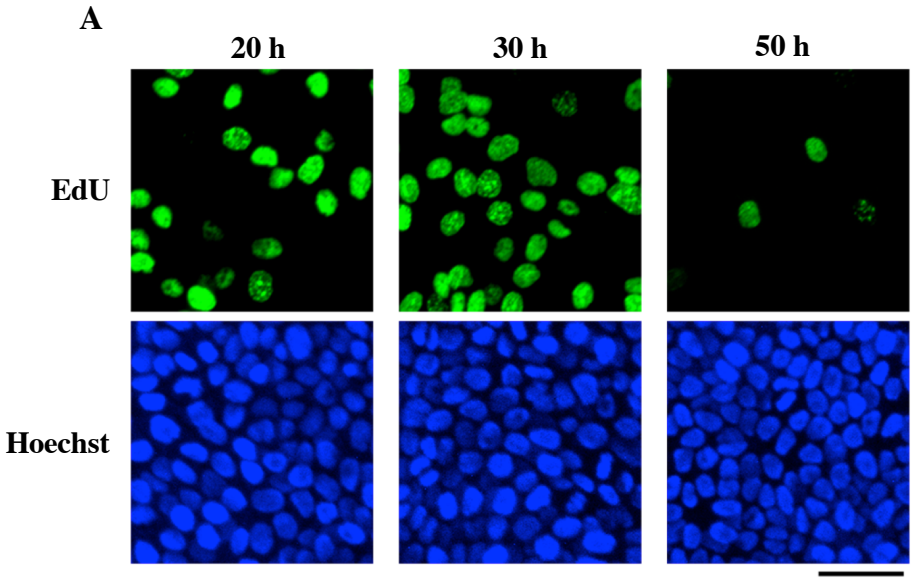

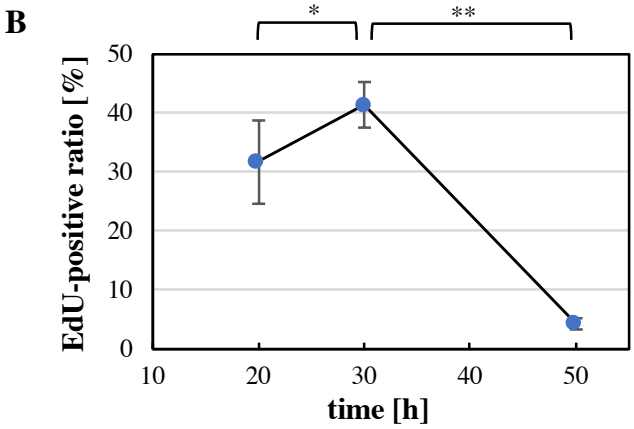

Figure S2. Time-dependent change in EdU incorporation into nuclei in keratinocyte sheets (Related to Figure 1). (A) EdU incorporation into nuclei in keratinocyte sheets that were grown for indicated time after seeding cells. Total nuclei were labeled with Hoechst. Scale bar: 50 μm. (B) Time-dependent change in the ratio of EdU-positive cells in keratinocyte sheets after seeding cells. Each data point represents mean ± SD. n = 7 (> 100 cells in each experiment). *$P < 0.05$; **$P < 0.01$ (Student's two-tailed, unpaired *t*-test).

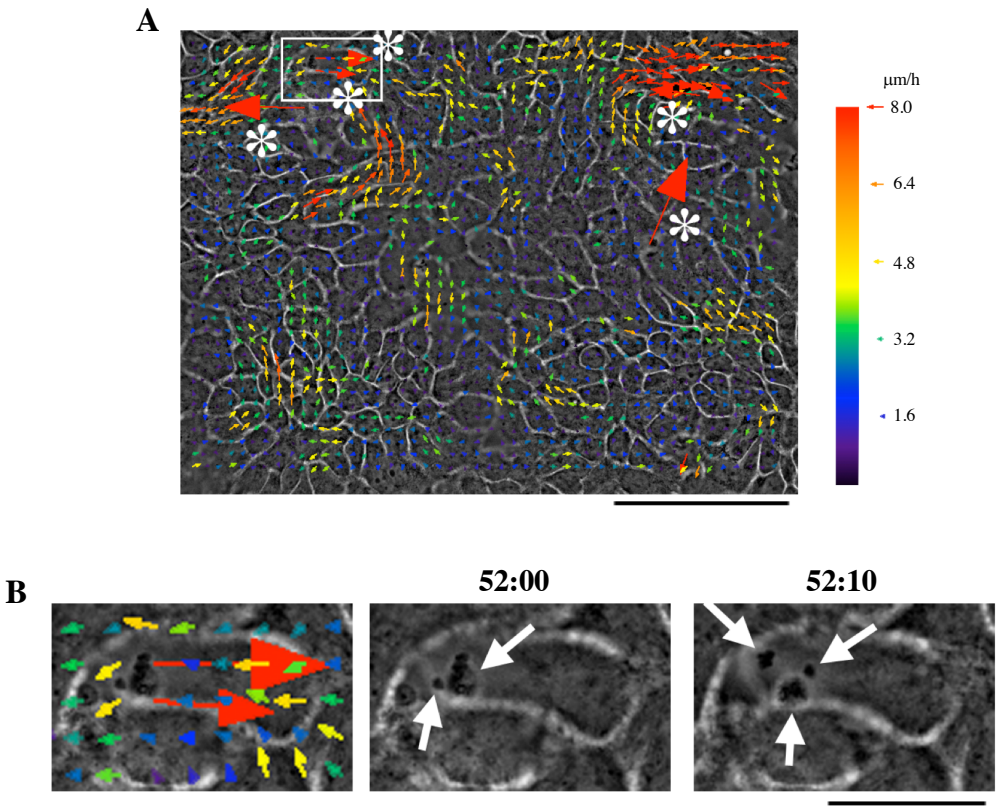

Figure S3. Floating extracellular particles cause appearance of aberrant vectors in PIV (Related to Figure 1). (A) A velocity vector map for a keratinocyte sheet at 52 h after seeding cells was overlaid to its phase contrast image. Aberrantly large vectors are indicated by asterisks. Scale bar: 100 μm. (B) Left panel: an enlarged image of the boxed region in (A). Middle and right panels: two consecutive phase contrast images (at time points of 52 h and 52 h 10 min after seeding cells) that were used for PIV calculation shown in (A). Only the region same as that in the left panel is shown. Floating extracellular particles are indicated by white arrows. See **Transparent Methods** for details. Scale bar: 30 μm.

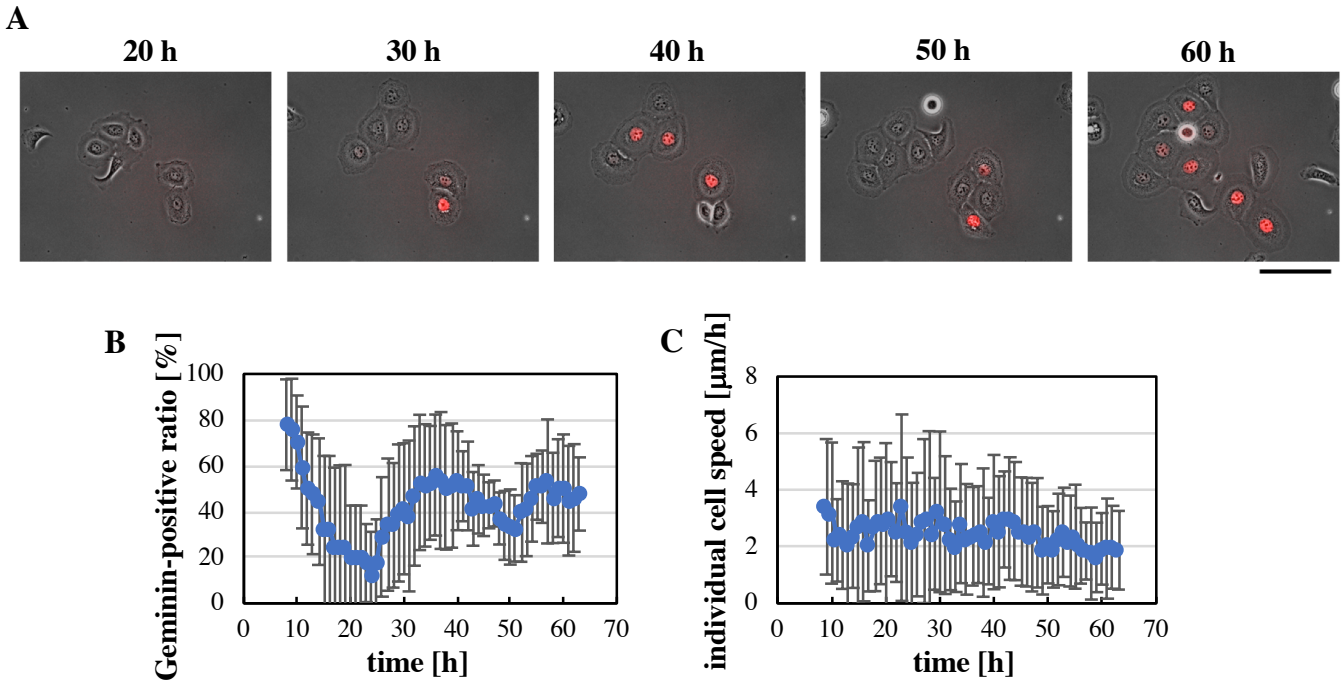

Figure S4. Time-dependent changes in cell cycle progression and cell motility in sparse keratinocytes (Related to Figures 1 and 6). (A) Geminin-based Fucci fluorescence images (red) at indicated time after seeding cells were overlaid to phase contrast images of sparse keratinocytes. Scale bar: 100 μm. (B and C) Time-dependent changes in the ratio of Geminin-positive cells against total cells (B) and the individual cell speed (C) in sparse keratinocytes after seeding cells. Each data point represents mean ± SD. n = 8 (≥ 5 cells at each time point in each experiment) in (B) and 33 in (C).

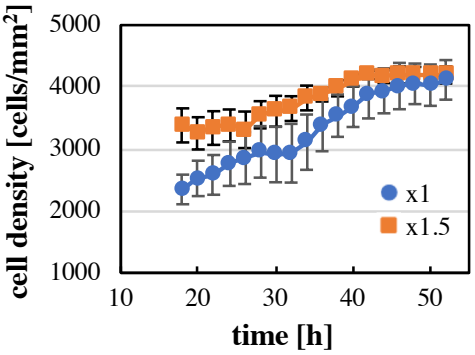

Figure S5. Time-dependent change of the cell density in H2B-GFP-expressing keratinocyte sheets after seeding different numbers of cells (Related to Figure 1). The numbers of seeded cells were 20 x 10^5 cells for 'x1' and 30 x 10^5 cells for 'x1.5'. Cell densities were quantified by counting H2B-GFP-labeled nuclei. Each data point represents mean ± SD. n = 3.

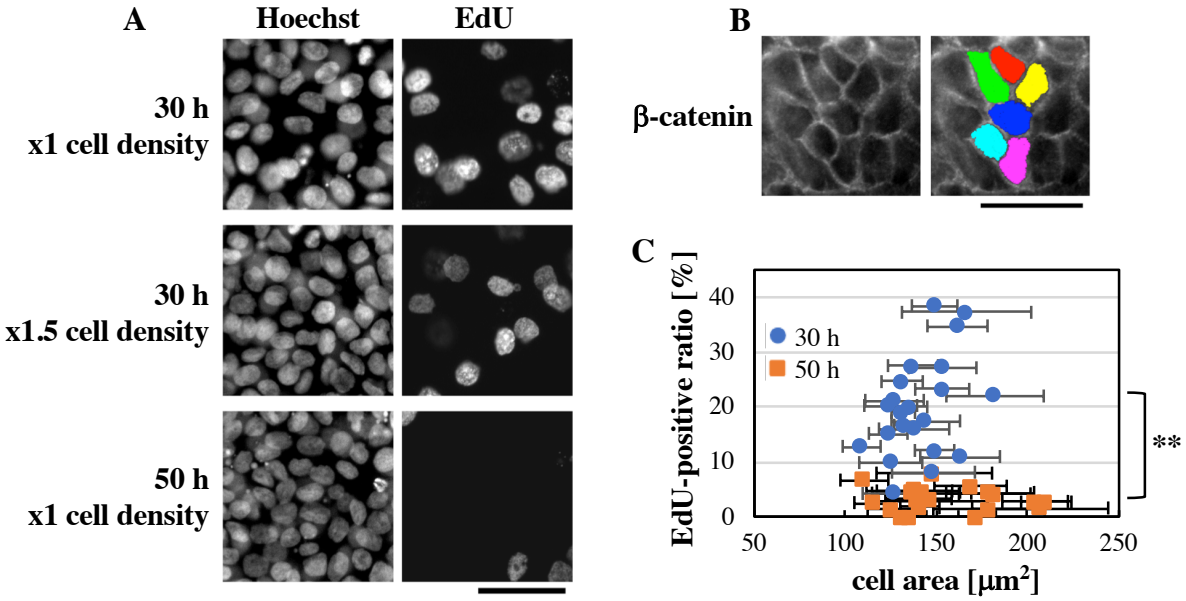

Figure S6. Effects of culture duration and cell density on nuclear incorporation of EdU in keratinocyte sheets (Related to Figure 1). (A) Keratinocyte sheets applied with EdU at the indicated time after seeding cells were fixed and stained for nuclei with Hoechst. The numbers of seeded cells were 20 x 10^5 cells for "x1" and 30 x 10^5 cells for "x1.5". Scale bar: 50 μm. (B) Measurement of individual cell areas in β-catenin-stained keratinocyte sheets. Scale bar: 50 μm. (C) Relationship between nuclear incorporation of EdU and the individual cell area in keratinocyte sheets at 30-h and 50-h time points after seeding cells. Individual cell areas and the ratio of EdU-positive cells were quantified in 22 regions (for "30 h") or 20 regions (for "50 h") of 3 keratinocyte sheets with different cell seeding densities, where each region contained > 50 cells. The individual cell area in each region is represented by mean ± SD. The ratio of EdU-positive cells at 30-h time point was significantly lower than that at 50-h time point (**P < 0.01; Student's two-tailed, unpaired t-test).

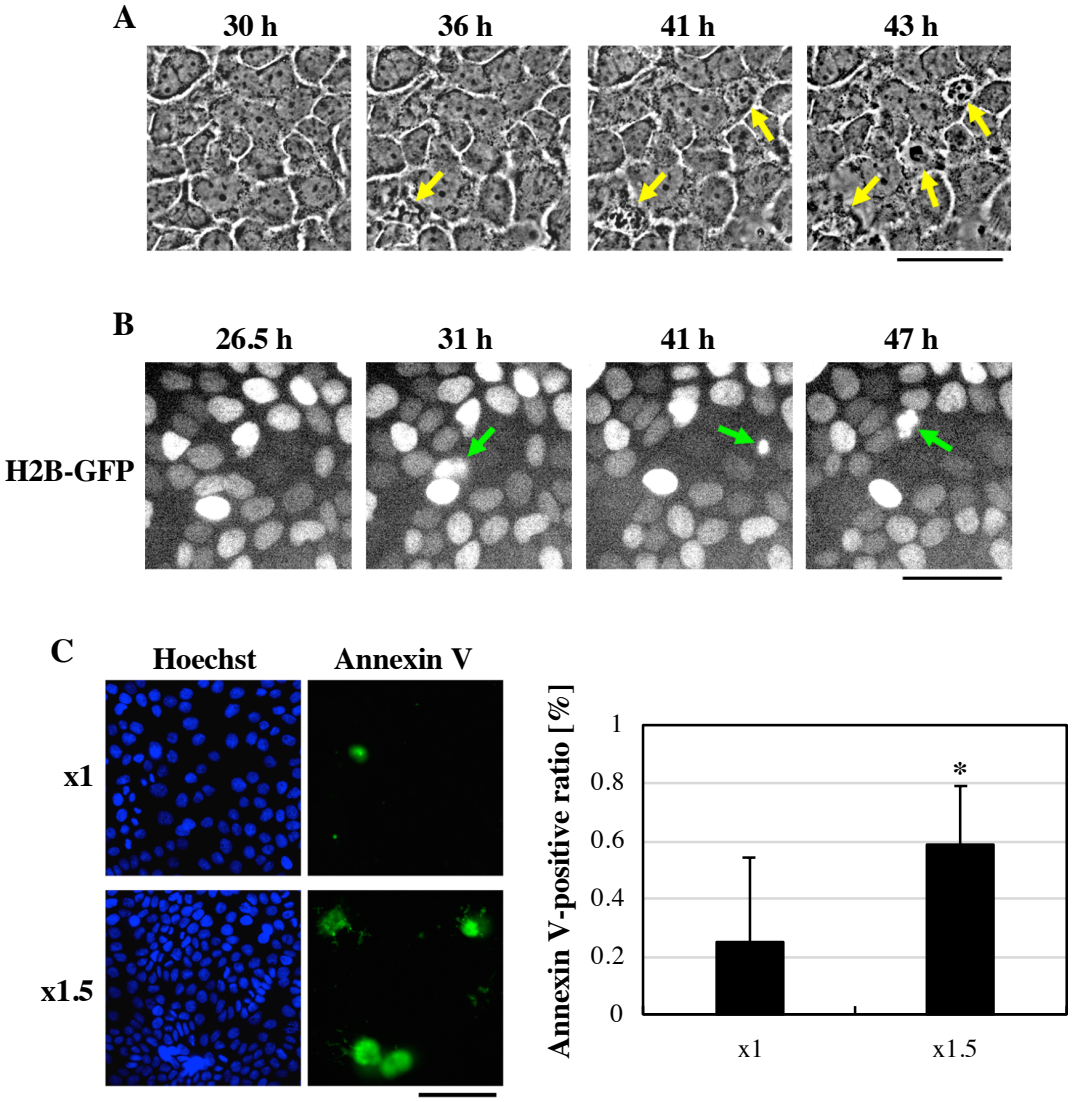

Figure S7. Cell death observed in the late time phase in keratinocyte sheets with a high cell seeding density (Related to Figure 1). (A) Phase contrast images of a keratinocyte sheet at indicated time points after seeding cells (30 x 10^5 cells seeded). Yellow arrows indicate dead cells. Scale bar: 50 μm. (B) Fluorescence images of an H2B-GFP-expressing keratinocyte sheet at indicated time points after seeding cells (30 x 10^5 cells seeded). Green arrows indicate dead cells with condensed nuclei. Scale bar: 50 μm. (C) Keratinocyte sheets with different cell seeding densities were grown for 40 h and treated with FITC-labelled Annexin V and Hoechst 33342. The numbers of seeded cells were 20 x 10^5 cells for "x1" and 30 x 10^5 cells for "x1.5". Left panels: fluorescence images of Hoechst-stained nuclei and cell-surface-bound Annexin V in the keratinocyte sheets. Scale bar: 100 μm. Right graph: the ratio of Annexin V-positive cells in the keratinocyte sheets. Each bar represents mean ± SD. n = 8 (> 300 cells each). *$P < 0.05$ (Student's two-tailed, unpaired *t*-test).

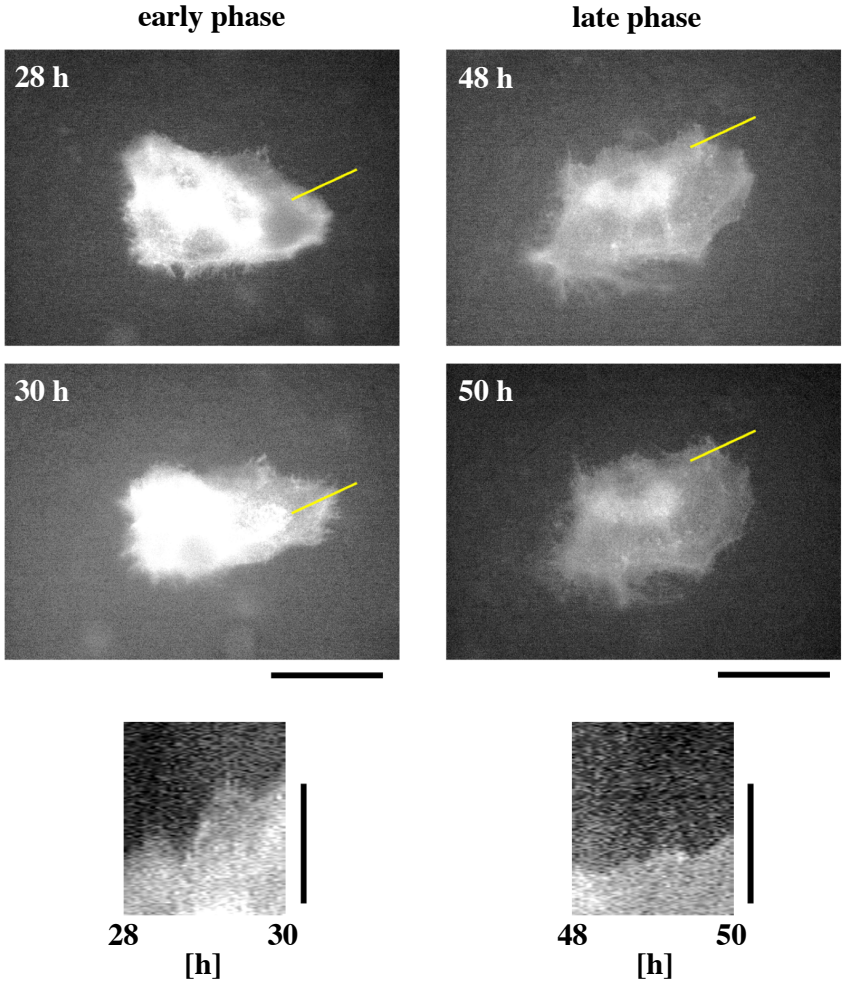

Figure S8. Kymograph analysis of the protrusive activity of keratinocytes in keratinocyte sheets (Related to Figure 2). HaCaT cells expressing F-tractin-GFP were sparsely mixed with naïve HaCaT cells and seeded to form a keratinocyte sheet. A single F-tractin-GFP-expressing cell in a sheet was tracked. Upper four panels show snapshots of an F-tractin-GFP-expressing cell at indicated time points after seeding cells. Lower two panels represent kymographs created along yellow lines in the upper snapshots. Protruding regions of the cell in early (from 28- to 30-h time points) and late (from 48- to 50-h time points) time phases were analyzed. Scale bars: 50 μm for snapshots and 20 μm for kymographs.

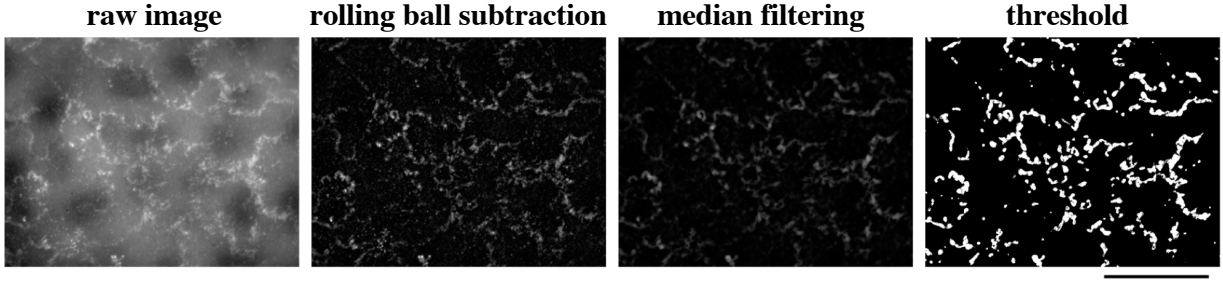

Figure S9. Image processing to extract cortactin-positive lamellipodia regions (Related to Figure 2). A immunofluorescence image of cortactin (raw image) was subjected to rolling ball subtraction of the background staining. Tiny dots outside wavy lamellipodia were then removed by median filtering. In the resultant image, lamellipodia regions were extracted by setting a threshold level. Scale bar: 30 μm.

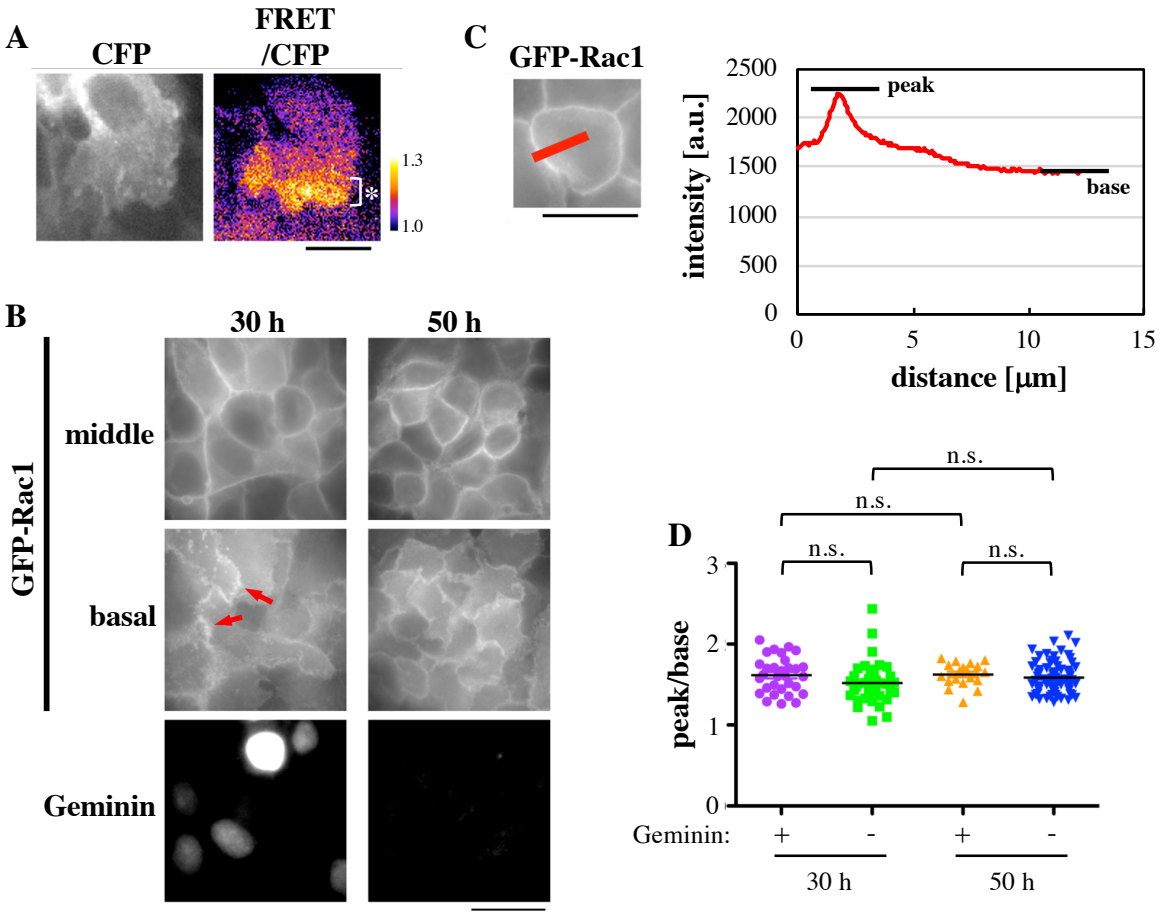

Figure S10. Localization of Rac1 in keratinocyte sheets (Related to Figure 2). (A) CFP and FRET/CFP ratio images of a RaichuEV-Rac-expressing keratinocyte in a keratinocyte sheet. An asterisk indicates the lamellipodia region with high Rac1 activity. Scale bar: 20 μm. (B) Keratinocyte sheets introduced with the Geminin-based Fucci probe and GFP-Rac1 were fixed and observed at 30-h and 50-h time points after seeding cells. For GFP-Rac1, middle and basal focal planes are shown. Red arrows indicate accumulation of GFP-Rac1 at lamellipodia tips. Scale bar: 30 μm. (C) The method for analyzing Rac1 localization at the cell-cell boundary. Fluorescence intensities of GFP-Rac1 along a line crossing the cell-cell boundary (red line in the left panel) were measured. Then, the peak intensity at the cell-cell boundary and the base intensity in the internal region of the cell were obtained (right graph). The ratio of the peak intensity against the base intensity was used as a index for relative localization of Rac1 at the cell-cell boundary. (D) The peak/base intensity ratio of GFP-Rac1 was calculated for cells grown for 30 h or 50 h after seeding cells. Geminin-positive cells and Geminin-negative ones were analyzed separately. n = 31 (30 h, Geminin-positive), 39 (30 h, Geminin-negative), 19 (50 h, Geminin-positive) and 69 (50 h, Geminin-negative). n.s., no significant difference (Student's two-tailed, unpaired *t*-test).

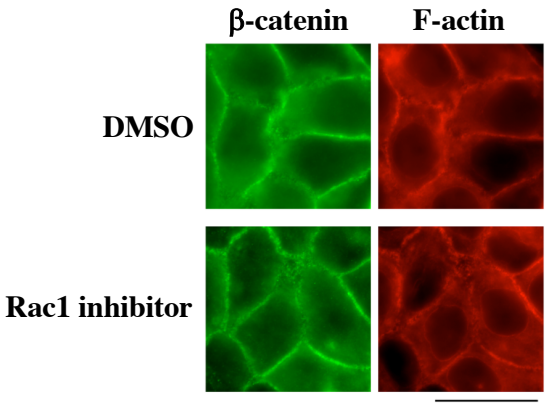

Figure S11. Effect of Rac1 inhibition on formation of adherens junctions (Related to Figure 3). Keratinocyte sheets formed in the presence of DMSO (control) or the Rac1 inhibitor (20 μM NSC23766) were fixed at 30 h after seeding cells and stained for β-catenin and F-actin. Scale bar: 30 μm.

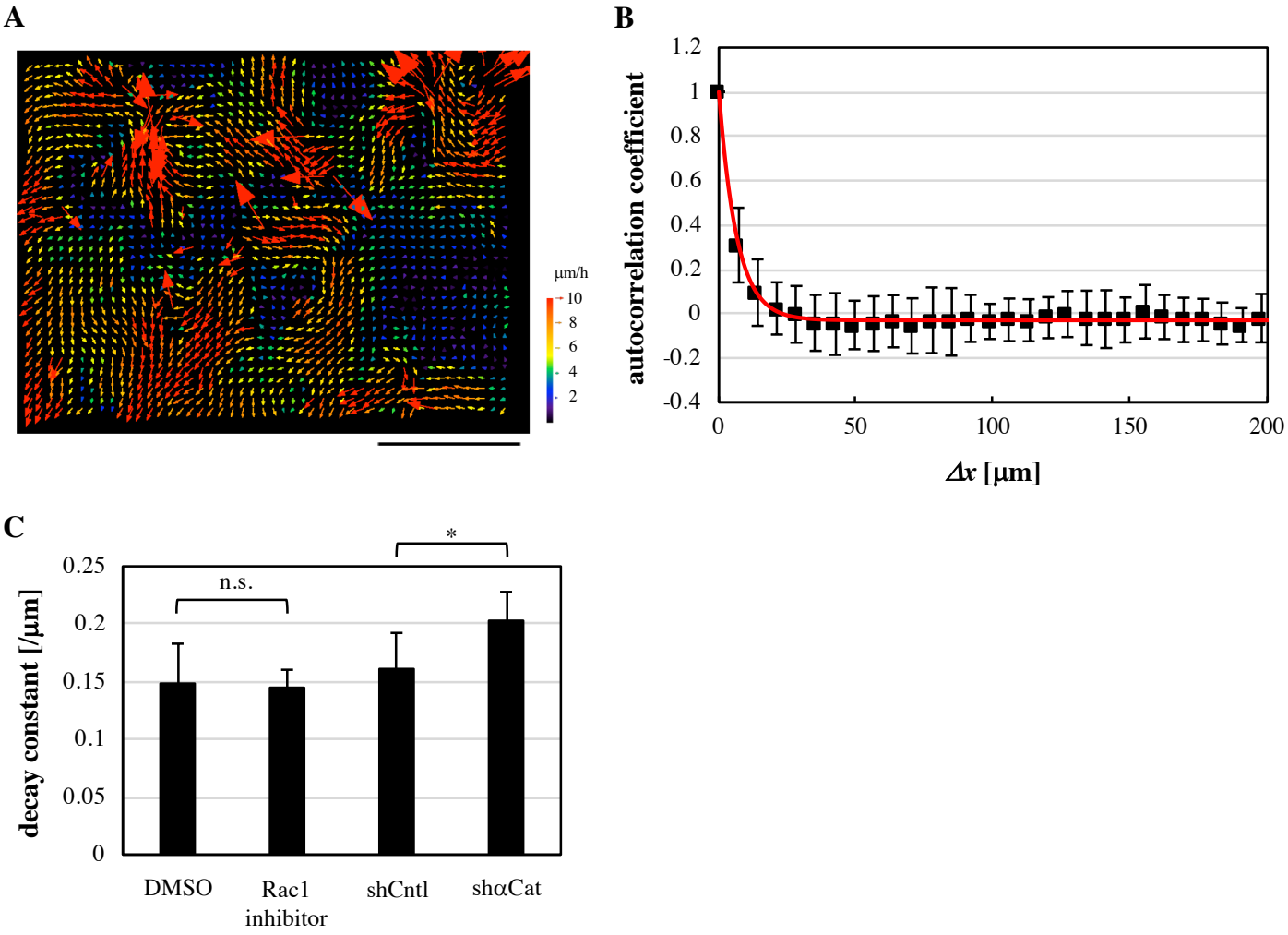

Figure S12. Spatial autocorrelation analysis of cell movement direction in keratinocyte sheets (Related to Figures 3 and 4). (A) A typical velocity vector map for keratinocyte sheets at 20 h after seeding cells. Scale bar: 100 μm. (B) Spatial autocorrelation for distribution of vector angles in the velocity vector map shown in (A) was analyzed. Correlogram of the spatial autocorrelation against Δx is shown. Each plot represents the averaged autocorrelation coefficient ± SD (n = 35). The plots were fitted with the equation [1] (red line). See **Transparent Methods** for details. (C) Decay constants in regression curves of correlograms with the equation [1] were calculated for keratinocyte sheets at 20 h after seeding cells. Keratinocyte sheets treated with the Rac1 inhibitor (20 μM NSC23766) or the vehicle only (DMSO), and keratinocyte sheets expressing shRNA against α-catenin (shαCat) or non-targeting shRNA (shCntl) were analyzed. The larger the decay constant is, the shorter the correlation length of spatial distribution of velocity vector angles is, and, therefore, the less collective the cell movement in the keratinocyte sheet is. Each bar represents mean ± SD. n = 6. *$P < 0.05$; n.s., no significant difference (Student's two-tailed, unpaired *t*-test).

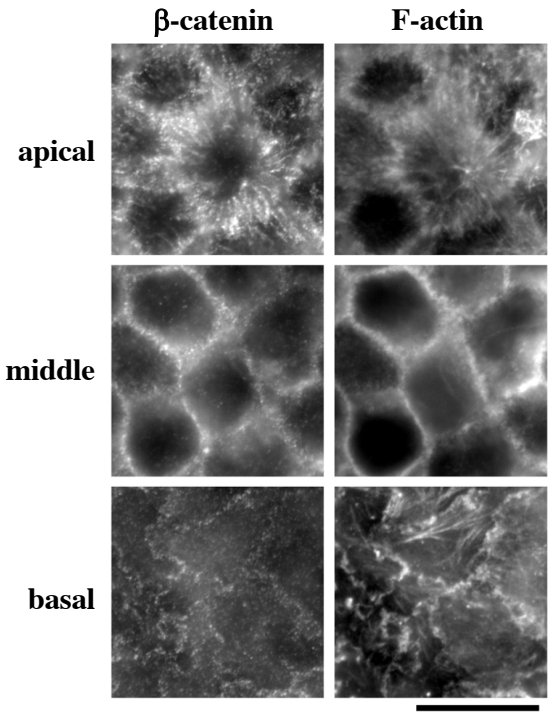

Figure S13. Assemblies of β-catenin and F-actin at different focal planes of a keratinocyte sheet (Related to Figure 4). A keratinocyte sheet at 50 h after seeding cells was stained for β-catenin and F-actin. Apical, middle and basal focal planes of the keratinocyte sheet are shown. Scale bar: 20 μm.

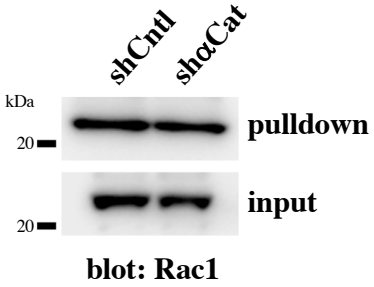

Figure S14. Depletion of α-catenin does not alter the Rac1 activity (Related to Figures 4 and 5). Keratinocyte sheets expressing shRNA against α-catenin (shαCat) or non-targeting shRNA (shCntl) were grown for 30 h after seeding cells. Their lysates were subjected to the PAK1-PBD-based pulldown assay for active Rac1.

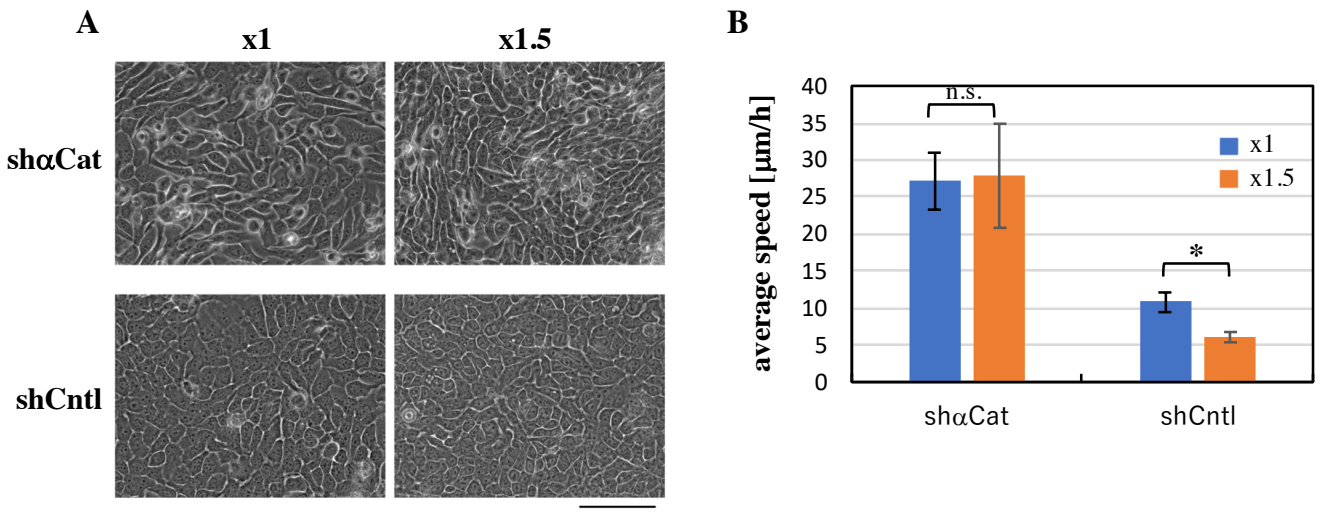

Figure S15. Effect of the cell seeding density on motility of α-catenin-depleted keratinocytes (Related to Figure 4). (A) Phase contrast images of HaCaT cells expressing shRNA against α-catenin (shαCat) or non-targeting shRNA (shCntl) that were seeded at different densities. Images at 20 h after seeding cells are shown. The numbers of seeded cells were 20 x 10^5 cells for "x1" and 30 x 10^5 cells for "x1.5". Scale bar: 100 μm. (B) Average speeds in α-catenin shRNA- or non-targeting shRNA-expressing keratinocyte sheets at 20 h after seeding cells. The numbers of seeded cells were 20 x 10^5 cells for "x1" and 30 x 10^5 cells for "x1.5". Each bar represents mean ± SD (n = 3). *$P < 0.05$; n.s., no significant difference (Student's two-tailed, unpaired *t*-test).

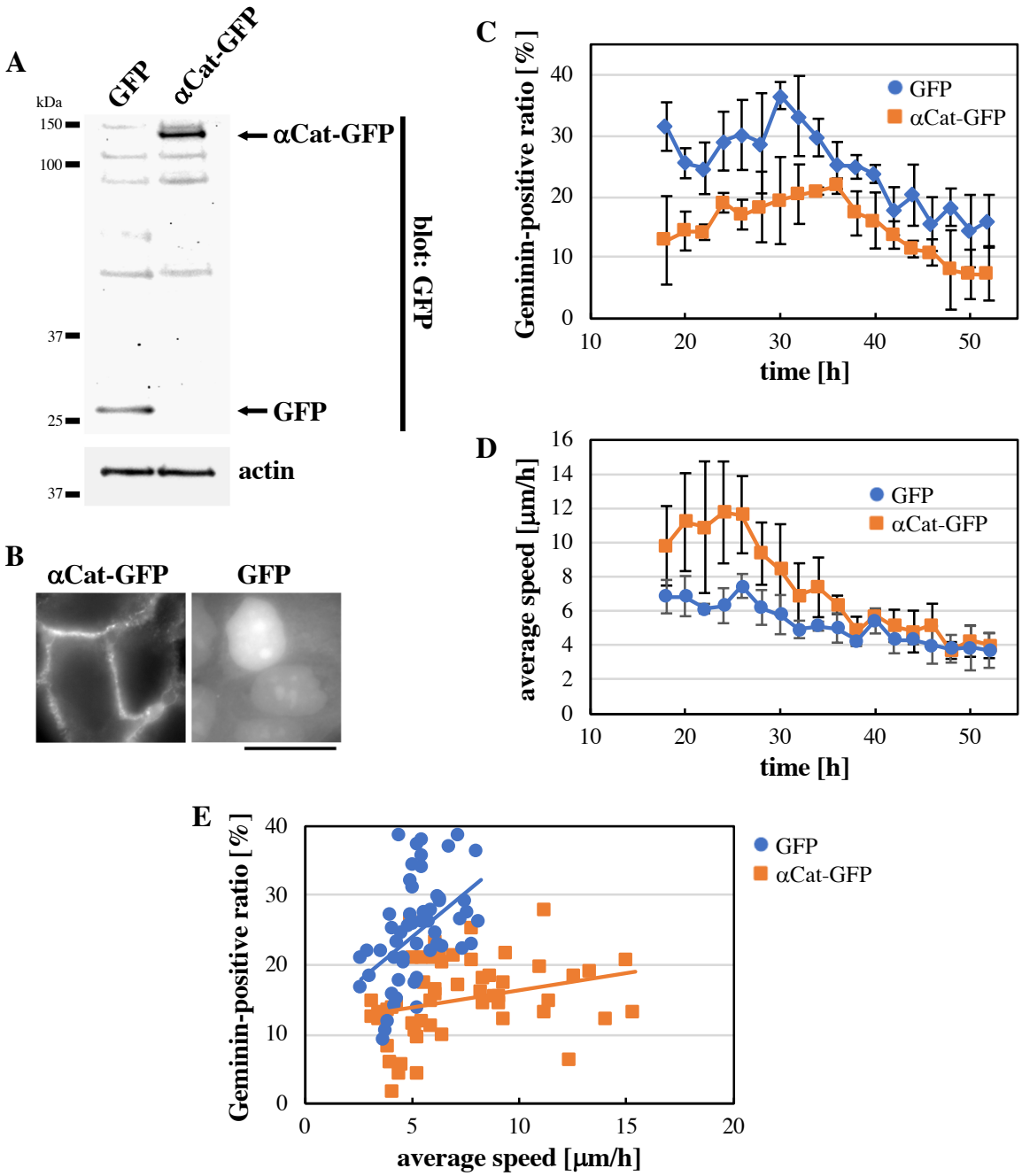

Figure S16. Effect of α-catenin overexpression on cell cycle progression and cell motility in keratinocyte sheets (Related to Figure 4). (A) Immunoblot analyses of expression of α-catenin-GFP (αCat-GFP) and GFP in HaCaT cells. (B) Fluorescence images of α-catenin-GFP (αCat-GFP) and GFP expressed in keratinocyte sheets. Images at 30 h after seeding cells are shown. Scale bar: 20 μm. (C and D) Time-dependent changes in the ratio of Geminin-positive cells (C) and the average speed (D) in keratinocyte sheets expressing α-catenin-GFP (αCat-GFP) or GFP after seeding cells. Each data point represents mean ± SD. n = 3 (> 100 cells at each time point in each experiment in (C)). (E) The ratio of Geminin-positive cells was plotted against the average speed in α-catenin-GFP (αCat-GFP)- or GFP-expressing keratinocyte sheets at each time point throughout observation. Data from three independent experiments were combined for each cell type. Regression lines of linear fitting are shown for both cell types.

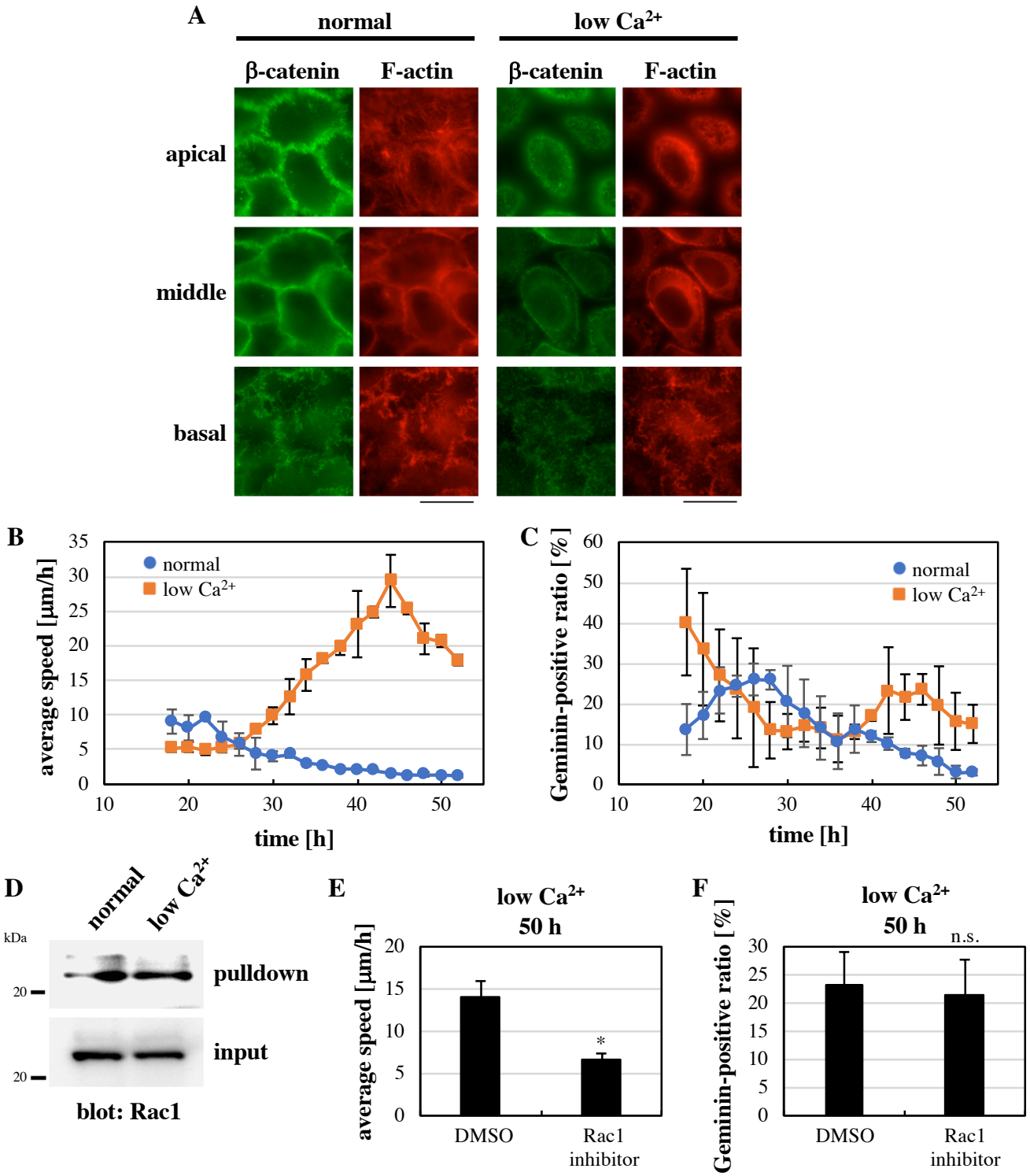

Figure S17. Effect of extracellular Ca^{2+} depletion on cell cycle progression and cell motility in keratinocyte sheets (Related to Figures 4 and 5). (A) Fluorescence images of β-catenin and F-actin at different focal planes of keratinocyte sheets at 50 h after seeding cells in the normal or low Ca^{2+} medium. Scale bars: 20 μm. (B and C) Time-dependent changes in the average speed (B) and the ratio of Geminin-positive cells (C) in keratinocyte sheets after seeding cells in the normal or low Ca^{2+} medium. (D) The Pak1-PBD-based pulldown assay for active Rac1. Lysates of keratinocyte sheets grown for 50 h after seeding cells in the normal or low Ca^{2+} medium were subjected to the assay. (E and F) The average speed (E) and the ratio of Geminin-positive cells (F) in keratinocyte sheets at 50 h after seeding cells in the normal or low Ca^{2+} medium. Each bar represents mean ± SD. n = 3 (> 100 cells in each experiment in (F)). *$P < 0.05$; n.s., no significant difference (Student's two-tailed, unpaired *t*-test).

Transparent Methods

Cell lines

Human HaCaT keratinocytes (Cell Lines Service) and HEK293T cells were maintained in high-glucose Dulbecco's modified Eagle's medium (Nacalai Tesque) supplemented with 10% fetal bovine serum (Thermo Fisher Scientific).

HaCaT cells expressing the Geminin-based Fucci fluorescent cell cycle probe, H2B-GFP, mEGFP-Rac1, mEGFP, or shRNA against α-catenin and/or non-targeting shRNA were generated using the retrovirus system. The retroviral vectors for expression of mEGFP-Rac1 and mEGFP were constructed by subcloning DNA sequences of human Rac1 (provided by Kozo Kaibuchi, Nagoya University, Japan) and/or mEGFP into the pMXs-IRES-Blasticidin plasmid (provided by Toshio Kitamura, University of Tokyo, Japan) (Kitamura et al., 2003). The pRetroX-SG2M-Red (Takara Bio), pMXs-IRES-Blasticidin-mEGFP-Rac1, pMXs-IRES-Blasticidin-mEGFP or pBabe.puro-H2B-GFP (provided by Keiko Kawauchi, Konan University, Japan) plasmid, or the pSUPER.retro.puro or pSUPER.retro.hygro plasmid carrying the sequence of either shRNA against human α-catenin or non-targeting shRNA (Hirata et al., 2017) was co-transfected with the pE-ampho plasmid into HEK293T cells using the GeneJuice transfection reagent (Merck). The HEK293T cell media containing viral particles were collected at 48 h after the transfection, filtered through 0.45-μm filters, and used for infection into HaCaT cells in the presence of 8 μg/ml polybrene (Sigma-Aldrich). Infected HaCaT cells were selected with 4 μg/ml puromycin (Sigma-Aldrich), 1000 μg/ml hygromycin B (Wako Pure Chemical) and/or 7 μg/ml blasticidin S hydrochloride (Wako Pure Chemical).

HaCaT cells expressing RaichuEV-Rac1 were generated using the piggyBac transposase system (Yusa et al., 2009). The expression vectors for RaichuEV-Rac1 (provided by Michiyuki Matsuda, Kyoto University, Japan) and piggyBac transposase (System Biosciences) were co-transfected into HaCaT cells using the GeneJuice transfection reagent. Transfected cells were selected with 7 μg/ml blasticidin S hydrochloride.

αE-catenin-EGFP (provided by Shigenobu Yonemura, Tokushima University, Japan) and EGFP were introduced into HaCaT cells by transfecting the cells with their expression vectors using the GeneJuice transfection reagent. Transfected cells were selected with 800 μg/ml G-418 (Sigma-Aldrich).

F-tractin-EGFP (Johnson and Schell, 2009) was introduced into HaCaT cells by transfecting the cells with its expression vector (provided by Michael J. Schell, Uniformed Services University, USA) using the GeneJuice transfection reagent.

Low Ca^{2+} medium

Ca^{2+}-free, high-glucose Dulbecco's modified Eagle's medium (Nacalai Tesque) was supplemented with 0.3 mM EGTA, 584 mg/l L-glutamine, 110 mg/l sodium pyruvate, 10% fetal bovine serum (Thermo Fisher Scientific). Given the concentration of Ca^{2+} in FBS to be 3.4 mM (Nagakura et al., 1987), the free Ca^{2+} concentration in the low Ca^{2+} medium was estimated as ~40 μM (calculated using Ca-EGTA Calculator v1.3 (Bers et al., 2010)).

Antibodies and chemicals

The mouse monoclonal antibody against cortactin (05-180) and the rabbit polyclonal antibody against Rac1 (07-1464) were obtained from Merck. The rabbit polyclonal antibody against α-catenin (C2018) and the mouse monoclonal antibody against β-actin (A5441) were from Sigma-Aldrich. The rabbit monoclonal antibody against E-cadherin (3195S) was from Cell Signaling Technology. The rabbit polyclonal antibody against β-catenin (ab6302) was from Abcam. Alexa Fluor 488-goat anti-mouse IgG and Alexa Fluor 488-goat anti-rabbit IgG antibodies, and Alexa Fluor 546-phalloidin were from Thermo Fisher Scientific. Horseradish peroxidase (HRP)-conjugated anti-mouse IgG and anti-ribbit IgG antibodies were from GE Healthcare. The Rac1 inhibitor NSC23766 was from Merck. Dimethyl sulfoxide (DMSO) was from Sigma-Aldrich.

Live cell imaging

HaCaT cells expressing the indicated fluorescent probe were seeded (20×10^5 cells for the "dense" condition and 0.3×10^5 cells for the "sparse" condition, otherwise specified) in the presence or absence of the indicated drug onto a 35-mm glass bottom dish (3910-035, AGC Techno Glass) precoated with 50 μg/ml collagen (Koken). Under the "dense" condition of cell seeding, the surface of the collagen-coated glass bottom dish was fully covered with cells. Just after seeding cells, the dish was placed in an observation chamber of the BioStation IM fluorescence microscope (Nikon) under the 37 °C and 5% CO_2 humidified atmosphere. Fluorescence and phase contrast images were captured at 30-min

(for imaging of F-tractin-EGFP, RaichuEV-Rac1 or H2B-GFP) or 10-min (for other cases) intervals. For RaichuEV-Rac1 imaging, the following filters and dichroic mirrors obtained from Nikon were used; the excitation filter FF02-438/24-25, the dichroic mirror FF458-Di02-25x36, and the emission filters FF01-542/27-25 (for FRET) and FF01-483/32-25 (for CFP).

EdU incorporation and immunofluorescence

For the EdU incorporation assay, HaCaT cells grown for the indicated duration after seeding cells in the presence or absence of the indicated drug were incubated for 2 h with 10 μM EdU in the presence or absence of the same drug. The cells were then fixed and permeabilized with 4% formaldehyde and 0.5% Triton X-100, respectively, in PBS, and incorporated EdU was visualized with Alexa Fluor 488-azide using the Click-iT technology (Thermo Fisher Scientific). Total nuclei were stained with 5 μg/ml Hoechst 33342 (Thermo Fisher Scientific).

Immunofluorescence staining was conducted as described previously (Hirata et al., 2008). In brief, cells were fixed and permeabilized for 30 min with 4% formaldehyde and 0.2% Triton X-100 in the cytoskeleton stabilizing buffer (137 mM NaCl, 5 mM KCl, 1.1 mM Na_2HPO_4, 0.4 mM KH_2PO_4, 4 mM $NaHCO_3$, 2 mM $MgCl_2$, 5.5 mM glucose, 2 mM EGTA and 5 mM PIPES, pH 6.1), which was followed by blocking with 1% BSA in the cytoskeleton stabilizing buffer for 30 min. The cells were then incubated with the primary antibody for 40 min, washed, and further incubated with the secondary antibody (and fluorescent phalloidin, when indicated) for 40 min.

Fluorescence images of fixed cells were obtained using an epi-fluorescence inverted microscope (ECLIPSE TE2000-U, Nikon) equipped with an air (NA 0.30, 10 ×; Plan Fluor, Nikon) or an oil immersion (NA 1.45, 100 ×; Plan Apo TIRF, Nikon) objective and a complementary metal oxide semiconductor camera (ORCA-Flash4.0 C11440-22CU, Hamamatsu Photonics). The Metamorph software (version 7.8, Molecular Devices) was used for image acquisition.

Annexin V staining

HaCaT cells were seeded (20×10^5 cells for "× 1" density and 30×10^5 cells for "× 1.5" density) onto 35-mm glass bottom dishes precoated with 50 μg/ml collagen. After culturing for 40 h, the cells were washed twice with PBS, and stained with FITC-

conjugated Annexin V (30018, Biorium) and Hoechst 33342 for 15 min at room temperature. The stained cells were observed with an epi-fluorescence microscope.

Image analyses

All image analyses were conducted using the public domain software ImageJ (version 1.45f).

The number of total cells was obtained by manually counting nuclei in either phase contrast, H2B-GFP or Hoechst 33342 images. Cells with nuclear Fucci fluorescence signal above the background intensity level were counted as Geminin-positive cells.

The velocity vector map in a confluent keratinocyte sheet was obtained by the PIV analysis (vector spacing of 16 pixels by 16 pixels) using the ImageJ plugin PIV (Tseng et al., 2012). Two consecutive frames (corresponding to 10-min time difference) of phase contrast time lapse images were used for each PIV calculation. The average speed in a velocity vector map was calculated by averaging the magnitude of velocity vectors in the map. Aberrantly large velocity vectors sometimes appeared in the PIV results (Figure S3A). Such aberrant vectors are likely to be caused by floating particles in the culture medium. The floating particles moved much faster than cells in keratinocyte sheets, and the large displacement of the particles during a single frame interval (i.e., 10 min) caused local errors in cross-correlation calculation between the frames, leading to appearance of 'spurious vectors' in PIV (Figure S3B). Importantly, the spurious vectors are minor among the calculated vectors (1680 vectors total) in a single PIV field, and appearance of spurious vectors did not affect dominantly the value of average speed in the field. For example, the average speed in Figure S3A was 2.67 μm/h with spurious vectors, and 2.57 μm/h after removing the spurious vectors.

Collectiveness of cell movement in a keratinocyte sheet was evaluated, as follows. The velocity vector map in a keratinocyte sheet at 20-h time point was obtained by the PIV analysis. Along a horizontal line (with a constant y value) in the map, spatial autocorrelation coefficients of velocity vector angles were calculated for different Δx values using the Real Statistics Resource Pack software (Release 6.6.1). The autocorrelation coefficients along all horizontal lines available in the map (35 lines) were averaged for each Δx value, and the correlogram against Δx was created using the averaged autocorrelation coefficients (Figure S12B). The correlogram was fitted with the equation,

$$A(\Delta x) = c \times \left(e^{-d \cdot \Delta x} - 1\right) + 1, \quad [1]$$

where $A(\Delta x)$ is the averaged autocorrelation coefficient at Δx, and c and d are fitting parameters (Figure S12B). The larger the decay constant d is, the shorter the correlation length of spatial distribution of velocity vector angles is, and, therefore, the less collective the cell movement in a keratinocyte sheet is.

The velocity of single cells under the sparse condition was measured by tracking the center of mass of nucleoli for each cell. The region of each nucleolus was determined by setting a threshold level in a phase contrast image. Time frames in which the cell was at the mitosis or cytokinesis stage were excluded from the analysis.

To analyze correlation between cell cycle progression and cell movement in a keratinocyte sheet, the Geminin-positive cells/total cells ratio was plotted against the average speed in the sheet at each time point throughout the observation period. The plots for three keratinocyte sheets were combined together, and the correlation coefficient and the regression line of the combined plots were calculated.

Cortactin-positive lamellipodia regions in an anti-cortactin immunofluorescence image were defined, as follows (Figure S9). After rolling ball subtraction (with the ball radius of 15 pixels) of the background staining, the fluorescence image of cortactin was subjected to median filtering (with the 10-pixel radius) to remove spotty signals outside wavy lamellipodia. In the resultant image, pixels in which the fluorescence intensity was above the threshold level were determined as lamellipodia regions.

Time-dependent changes in the membrane protrusion activity of cells were analyzed using time lapse images of F-tractin-EGFP-expressing cells. After rolling ball subtraction (with the ball radius of 150 pixels) of the background intensity, the region of a cell in which the fluorescence intensity was above a threshold level was determined in each frame. By comparing the cell region in one frame with that in the immediately preceding frame, extended regions of the cell during the time interval (30 min) were identified.

The cell division tree analysis was conducted, as follows. Cells in a phase contrast image at 20 h after seeding cells were randomly chosen as “founders”, and they and their offspring were manually traced until 52 h after the seeding. Cells that escaped from the field of view during the trace were excluded from the analysis. Time points of division of founder cells and their offspring were recorded to construct cell division trees for individual founders. The number of offspring cells derived from each founder cell was

counted at 52 h after seeding cells. If a certain founder cell does not divide until 52 h after the seeding, the number of its offspring becomes one.

Pulldown assay

Specified types of HaCeT cells were seeded (16×10^6 cells for the "dense" condition and 2.4×10^5 cells for the "sparse" condition) onto collagen-coated 10-cm dishes in either normal DMEM or the low Ca^{2+} medium in the presence or absence of the indicated drug, and were grown for the indicated time period. After washing cells with cold PBS, the PAK1-PBD-based pulldown assay for active Rac1 was conducted using the Rac1 activation magnetic beads pulldown assay kit (17-10393, Merck). In brief, the cells were lysed with the Mg^{2+} lysis/wash buffer (MLB) that contained the protease inhibitor cocktail (Cytoskeleton), and centrifuged at 14,000 g for 5 min. The supernatants were used as the cell lysates for further procedures. The cell lysates were incubated with PAK1-PBD-coupled magnetic beads for 45 min at 4 ºC. The beads were washed three times with MLB, and, then, the precipitated proteins were eluted with 2 × lithium dodecyl sulfate sample buffer (Thermo Fisher Scientific) containing 2.5% β-mercaptoethanol (Sigma-Aldrich). The pulldown samples were subjected to the immunoblot analysis for Rac1.

Immunoblot

Cells were lysed with 2 × lithium dodecyl sulfate sample buffer containing 2.5% β-mercaptoethanol. The lysate was resolved by SDS-PAGE (4-12% Bis-Tris gel; Thermo Fisher Scientific), transferred onto the polyvinylidene fluoride membrane (Merck), and probed with primary and HRP-conjugated secondary antibodies. Imuno-reactive bands were detected with Chemi-Lumi One Super (Nacalai Tesque).

Supplemental References

Bers, D.M., Patton, C.W., and Nuccitelli, R. (2010). A practical guide to the preparation of Ca^{2+} buffers. Methods Cell Biol. *99,* 1-26.

Hirata, H., Samsonov, M., and Sokabe, M. (2017). Actomyosin contractility provokes contact inhibition in E-cadherin-ligated keratinocytes. Sci. Rep. *7,* 46326.

Hirata, H., Tatsumi, H., and Sokabe, M. (2008). Mechanical forces facilitate actin polymerization at focal adhesions in a zyxin-dependent manner. J. Cell Sci. *121,* 2795-2804.

Johnson, H.W., and Schell, M.J. (2009). Neuronal IP_3 3-kinase is an F-actin-bundling protein: role in dendritic targeting and regulation of spine morphology. Mol. Biol. Cell *20,* 5166-5180.

Kitamura, T., Koshino, Y., Shibata, F., Oki, T., Nakajima, H., Nosaka, T., and Kumagai, H. (2003). Retrovirus-mediated gene transfer and expression cloning: powerful tools in functional genomics. Exp. Hematol. *31,* 1007-1014.

Nagakura, K., Ueno, M., Brookins, J., Beckman, B.S., and Fisher, J.X. (1987). Effects of low calcium levels on erythropoietin production by human renal carcinoma cells in culture. Am. J. Physiol. *253,* C797-C801.

Tseng, Q., Duchemin-Pelletier, E., Deshiere, A., Balland, M., Guillow, H., Filhol, O., and Théry, M. (2012). Spatial organization of the extracellular matrix regulates cell-cell junction positioning. Proc. Natl. Acad. Sci. U.S.A. *109,* 1506-1511.

Yusa, K., Rad, R., Takeda, J., and Bradley, A. (2009). Generation of transgene-free induced pluripotent mouse stem cells by the piggyBac transposon. Nat. Methods *6,* 363-369.